Net Enthalpy Transport in Pulse Tube Refrigerators

Young Goo Kang* and Eun Soo Jeong**

Key Words : Pulse tube refrigerator, Net enthalpy flow, Enthalpy streaming, Mass streaming, Axial temperature gradient, Two-dimensional analysis

Abstract

Enthalpy transport in a pulse tube was investigated by two-dimensional analysis of mass, momentum and energy equations assuming that the axial temperature gradient in the pulse tube was constant. The time-averaged second-order conservation equations of mass, momentum and energy were used to show the existence of steady mass and enthalpy streaming. Effects of the axial temperature gradient, velocity amplitude ratio, and heat transfer between the gas and the tube wall on the steady mass and enthalpy streaming were shown. Enthalpy loss due to the steady mass streaming is zero for basic and orifice pulse tube refrigerators, but it is proportional to the axial temperature gradient and steady mass flow rate through a pulse tube for double inlet pulse tube refrigerators.

Nomenclature

A : Cross-sectional area of a pulse tube
C_p : Specific heat for constant pressure
H : Half of the distance between the parallel plates
$\langle \dot{H} \rangle$: Net enthalpy flow
$\langle \dot{H} \rangle_{id}$: Ideal net enthalpy flow by first-order velocity and temperature
$\langle \dot{H} \rangle_{st}$: Net enthalpy flow by steady mass streaming
i : Imaginary unit [$=\sqrt{-1}$]
k : Thermal conductivity
L : Length of a pulse tube
M_{total} : Total mass in a pulse tube
$\dot{m}$: Mass flow rate
Ma : Mach number [$=\omega s_1/\sqrt{\gamma R T_H}$]
p : Pressure
Pr : Prandtl number

* Sindo Ricoh, 277-22 Sungsudong, Sungdong ku, Seoul 133-705, Korea
** Dept. of Mechanical Engineering, Hongik University, 72-1 Sangsudong, Mapoku, Seoul121-791, Korea

R : Gas constant
s_1 : Displacement length of gas at $x=0$
s_2 : Displacement length of gas at $x=L$
T : Temperature
T_H : Temperature of hot heat exchanger
t : Time
u : Velocity component parallel to the wall
$\bar{u}$: Cross-sectional average of u
v : Velocity component perpendicular to the wall
x : Coordinate parallel to the wall
y : Coordinate perpendicular to the wall

Greek Letters

ϕ : Velocity phase angle
γ : Specific heat ratio
μ : Viscosity
ρ : Density
ω : Angular velocity

Superscripts

$*$: Dimensionless variable

Subscripts

0 : Values for zero axial temperature gradient
1 : First-order
2 : Second-order
m : Mean value
s : Steady component of the second-order solution

1. Introduction

Pulse tube refrigerators have been extensively studied in recent years due to their high reliability, structural simplicity, and low vibration at the cold end. Since the invention of the pulse tube refrigerator by Gifford and Longsworth[1] in the early 1960s, much work has been done to investigate and optimize the devices of this kind. A major improvement in the performance was achieved by Mikulin et al.,[2] who provided the closed end of the pulse tube with an orifice connected to a reservoir. Other modifications of the pulse tube refrigerators, such as double inlet type and four-valve type pulse tube refrigerators, have been suggested to improve the performance and to lower the cooling temperature.[3-7]

Since the refrigeration effect of a pulse tube refrigerator is generated by the net enthalpy flow in a pulse tube, it is essential to understand the flow and thermodynamic behaviors of the working gas in a pulse tube to improve the performance of a pulse tube refrigerators. A secondary flow was observed as steady large scale streaming for both basic and orifice pulse tube refrigerator configurations by Lee et al., and they showed that the enthalpy flow associated with the secondary streaming could be a major loss mechanism.[8] The one-dimensional enthalpy flow models, which have been widely used for the performance analysis of a pulse tube refrigerator, neglect the heat transfer between the working gas and the tube wall and momentum diffusion. Hence, they cannot show the existence of the secondary flow observed by Lee et al.[8] Two-or three-dimensional analysis should be done to investigate the effect of the secondary flow on the net enthalpy flow within a pulse tube.

Jeong and Smith[9] analysed momentum and heat transfers in a basic pulse tube refrigerator configuration with zero axial temperature gradient and showed that there existed a steady ci-

rculating secondary flow. Jeong[10] obtained the analytic solution of the steady component of the second-order axial velocity in a basic pulse tube refrigerator for small axial temperature gradient and thin boundary layer thickness, and showed the effect of the axial temperature gradient on the secondary flow. Lee et al.[11] proposed a numerical model for large axial temperature gradient and obtained the second-order velocity and temperature within a basic pulse tube refrigerators. Lee et al.[12] applied a two-dimensional model for the pulse tube of a orifice pulse tube refrigerator with zero axial temperature gradient. They showed the existence of steady mass streaming and the effect of heat transfer between the working gas and the tube wall on the net enthalpy flow. Liang et al.[13] proposed the compound pulse tube model in which the working gas in a pulse tube was divided into two parts: thermal viscous layer near the tube wall and the central region where heat and momentum diffusion could be neglected.

In this paper, two-dimensional analysis of a pulse tube was done assuming that the axial temperature gradient is constant. Fist-order solutions of continuity, momentum, and energy equations were obtained. From the steady second-order governing equations, which were obtained by time-averaging the second-order equations, the existence of the steady mass and enthalpy streaming was revealed. Effects of the axial temperature gradient, velocity amplitude ratio and heat transfer between the gas and the tube wall on the steady mass and enthalpy streaming were investigated.

2. Analysis Model and Governing Equations

Our attention will be restricted to the gas

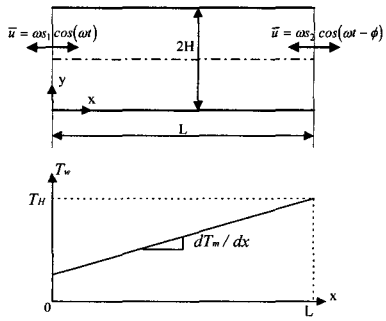

Fig.1 Schematic diagram of a pulse tube and wall temperature profile.

between the parallel plates as shown in Fig.1. Although the working spaces of pulse tubes have a shape of circular cylinder, parallel plates are chosen to simplify this analysis. $x=0$ denotes the interface between a pulse tube and a cold heat exchanger, and $x=L$ is the interface between a pulse tube and a hot heat exchanger. The plates have constant axial temperature gradient in x-direction, dT_m/dx. Sin ce the hot heat exchanger temperature of pulse tube refrigerators does not vary much during operation, the temperature at $x=L$, T_H, is assumed to be constant. The working gas oscillates with angular velocity ω. The cross-sectional averages of the displacement lengths of the working gas at $x=0$ and $x=L$ are s_1 and s_2, respectively. The velocity phase angle is ϕ.

The main assumptions used in the analysis are as follows:

(1) The amplitudes of the displacement lengths, s_1 and s_2, are far smaller than the length of a pulse tube, L.

(2) The gap between the plates, $2H$, is smaller than the pulse tube length, L. Hence, the temperature and velocity gradients in $x-$di rection are negligible compared to those in $y-$ direction. Also, the pressure is uniform in a

cross-section of a pulse tube.

(3) The temperatures of the plates do not vary with time since the heat capacities of the plates are far larger than that of the gas. In the absence of oscillation, the plates and the gas contained in them have a common temperature, T_m, which is a function of x.

(4) Physical properties of the working gas, such as viscosity, thermal conductivity and specific heat for constant pressure, are constant.

(5) The working gas is a perfect gas, and the flow is laminar.

2.1 First-order solutions

Conservation equations of mass, momentum and energy as well as the equation of state obtained under the above assumptions are described in Jeong.(10) The variables are non-dimensionalized as follows.

$$x^*=\frac{x}{L} \quad y^*=\frac{y}{H} \quad t^*=\frac{t}{1/\omega}$$
$$u^*=\frac{u}{\omega s_1} \quad v^*=\frac{v}{\omega s_1 H/L} \tag{1}$$
$$T^*=\frac{T}{T_H} \quad p^*=\frac{p}{p_0} \quad \rho^*=\frac{\rho}{\rho_0}$$

Here, p_0 and ρ_0 are the pressure and the density of the working gas when the axial temperature gradient, dT_m/dx, is zero. Dimensionless first-order solutions of velocity, temperature and density are expressed as follows. Only the real parts of first-order solutions have physical meaning.

$$u_1^*(x^*,y^*,t^*)=i\frac{s_1/L}{\gamma Ma^2}\frac{1}{\rho_m^*}\frac{dp_1^*}{dx^*}\left\{1-A(\beta,y^*)\right\} \tag{2}$$

$$v_1^*(x^*,y^*,t^*)=i\frac{s_1/L}{\gamma Ma^2}\frac{1}{\rho_m^*}\frac{d^2p_1^*}{dx^{*2}}\Big[-y^*$$
$$+E(\beta)-\frac{C(\beta,y^*)}{(1+i)\beta}\Big]$$
$$+i\frac{s_1/I}{\gamma Ma}\frac{1}{p_m^*}\frac{dT_m^*}{dx^*}\frac{dp_1^*}{dx^*}[-y^*+G(\beta,y^*)]$$
$$+i\frac{1}{\gamma(s_1/L)}\frac{p_1^*}{p_m^*}\Big[-y^*-(\gamma-1)\{F(\beta)$$
$$-\frac{D(\beta,y^*)}{(1+i)\beta\sqrt{\Pr}}\}\Big] \tag{3}$$

$$T_1^*(x^*,y^*,t^*)=\frac{\gamma-1}{\gamma}\frac{p_1^*}{p_m^*}\{1-B(\beta,y^*)\}$$
$$-\frac{1}{\gamma Ma^2}\left(\frac{s_1}{L}\right)^2\frac{1}{\rho_m^*}\frac{dT_m^*}{dx^*}\frac{dp_1^*}{dx^*}\{1$$
$$-\frac{\Pr}{1-\Pr}A(\beta,y^*)+\frac{1}{\Pr-1}B(\beta,y^*)\Big\} \tag{4}$$

$$\rho_1^*(x^*,y^*,t^*)=\frac{p_1^*}{\gamma T_m^*}\{1+(\gamma-1)B(\beta,y^*)\}$$
$$+\frac{1}{\gamma Ma^2}\left(\frac{s_1}{L}\right)^2\frac{1}{T_m^*}\frac{dT_m^*}{dx^*}\frac{dp_1^*}{dx^*}\{1$$
$$-\frac{\Pr}{1-\Pr}A(\beta,y^*)+\frac{1}{\Pr-1}B(\beta,y^*)\Big\} \tag{5}$$

Dimensionless first-order pressure can be written as $p_1^*(x^*,t^*)=\hat{p}_1^*(x^*)e^{it^*}$. The wave equation of the first-order pressure can be written as[11]

$$\frac{d}{dx^*}\left[\{1-E(\beta)\}\frac{d\hat{p}_1^*}{dx^*}\right]+\Big\{1-\frac{\Pr}{\Pr-1}E(\beta)$$
$$+\frac{1}{\Pr-1}F(\beta)\Big\}\frac{1}{T_m^*}\frac{dT_m^*}{dx^*}\frac{d\hat{p}_1^*}{dx^*}$$
$$+\frac{Ma^2}{(s_1/L)^2}\{1+(\gamma-1)E(\beta)\}\frac{\hat{p}_1^*}{T_m^*}=0 \tag{6}$$

Here,

$$\beta=\frac{H}{\sqrt{2\mu/(\rho_m\omega)}}=\beta_0\sqrt{\rho_m^*} \tag{7}$$

$$\beta_0=\frac{H}{\sqrt{2\mu/(\rho_0\omega)}} \tag{8}$$

$$A(\beta,y^*)=\frac{\cosh[(1+i)\beta(1-y^*)]}{\cosh[(1+i)\beta]} \tag{9}$$

$$B(\beta, y^*) = \frac{\cosh[(1+i)\beta\sqrt{\Pr}(1-y^*)]}{\cosh[(1+i)\beta\sqrt{\Pr}]} \tag{10}$$

$$C(\beta, y^*) = \frac{\sinh[(1+i)\beta(1-y^*)]}{\cosh[(1+i)\beta]} \tag{11}$$

$$D(\beta, y^*) = \frac{\sinh[(1+i)\beta\sqrt{\Pr}(1-y^*)]}{\cosh[(1+i)\beta\sqrt{\Pr}]} \tag{12}$$

$$E(\beta) = \frac{\tanh[(1+i)\beta]}{(1+i)\beta} \tag{13}$$

$$F(\beta) = \frac{\tanh[(1+i)\beta\sqrt{\Pr}]}{(1+i)\beta\sqrt{\Pr}} \tag{14}$$

$$G(\beta, y^*) = \frac{3\Pr-1}{2(\Pr-1)}\left\{E(\beta) - \frac{C(\beta, y^*)}{(1+i)\beta}\right\} - \frac{1}{\Pr-1}\left\{F(\beta) - \frac{D(\beta, y^*)}{(1+i)\beta\sqrt{\Pr}}\right\} - \frac{\tanh[(1+i)\beta]}{2} C(\beta, y^*) + \frac{(1-y^*)}{2} A(\beta, y^*) - \frac{1}{2\{\cosh[(1+i)\beta]\}^2} \tag{15}$$

The boundary conditions of the wave equation (6) can be obtained from the boundary conditions of the first-order axial velocity(equation (2)).

$$\frac{d\hat{p}_1^*}{dx^*}(x^*=0, t^*) = -\frac{i\rho_m^*\gamma Ma^2}{(s_1/L)\{1-E(\beta)\}} \tag{16}$$

$$\frac{d\hat{p}_1^*}{dx^*}(x^*=1, t^*) = -\frac{i\rho_m^*\gamma Ma^2(s_2/s_1)}{(s_1/L)\{1-E(\beta)\}} e^{-i\phi} \tag{17}$$

For constant axial temperature gradient, dT_m/dx, the mean temperature of the gas is expressed as $T_m(x) = T_H - dT_m/dx \times (L-x)$. Using the ideal gas relation, total mass of the working gas within a pulse tube can be obtained as

$$M_{total} = \frac{p_m A}{R} \frac{1}{dT_m/dx} \ln\left(\frac{T_H}{T_H - (dT_m/dx)L}\right) \tag{18}$$

where A is the cross-sectional area of a pulse tube. For zero axial temperature gradient, total mass of the working gas is given as follows.

$$M_{total} = \int_0^L \rho_0 A dx = \frac{p_0 AL}{RT_H} \tag{19}$$

Dimensionless mean pressure can be obtained from the assumption that total mass of the working gas within a pulse tube is constant.

$$p_m^* = \frac{p_m}{p_0} = -\frac{dT_m^*/dx^*}{\ln(1 - dT_m^*/dx^*)} \tag{20}$$

Dimensionless mean density is obtained from the ideal gas relation as

$$\rho_m^*(x^*) = -\frac{1}{T_m^*(x^*)} \frac{dT_m^*/dx^*}{\ln(1 - dT_m^*/dx^*)} \tag{21}$$

2.2 Time-averaged second-order mass, momentum and energy conservation equations

Time-averaged second-order conservation equations of mass and momentum can be written as follows.(10)

$$\frac{\partial(\rho_m^* u_s^*)}{\partial x^*} + \rho_m^* \frac{\partial v_s^*}{\partial y^*} = -\frac{\partial \langle \rho_1^* u_1^* \rangle}{\partial x^*} - \frac{\partial \langle \rho_1^* v_1^* \rangle}{\partial y^*} \tag{22}$$

$$\frac{\partial^2 u_s^*}{\partial y^{*2}} = 2\frac{\beta_0^2}{\gamma Ma^2} \frac{s_1}{L} \frac{dp_s^*}{dx^*} + 2\beta_0^2 \frac{s_1}{L} \rho_m^* \left\langle u_1^* \frac{\partial u_1^*}{\partial x^*} \right\rangle + 2\beta_0^2 \frac{s_1}{L} \rho_m^* \left\langle v_1^* \frac{\partial u_1^*}{\partial y^*} \right\rangle + 2\beta_0^2 \left\langle \rho_1^* \frac{\partial u_1^*}{\partial t^*} \right\rangle \tag{23}$$

where angular bracket(< >) denotes time-averaging. u_s^* and v_s^* are the steady components of the dimensionless velocities in x and y directions, respectively. p_s^* is the steady component of the dimensionless second-order pressure.

Integrating equation (22) from $y^*=0$ to

$y^*=1$ gives the following equation since $v_s^*=0$ and $v_1^*=0$ at $y^*=0$ and $y^*=1$.

$$\frac{\partial}{\partial x^*}\int_0^1[\rho_m^* u_s^* + \langle \rho_1^* u_1^* \rangle]dy^* = 0 \tag{24}$$

Dimensionless net mass flow rate can be obtained by integrating equation (24) with respect to x^*.

$$\dot{m}_s^* = \frac{\dot{m}_s}{\rho_0 \omega s_1 H} = \int_0^1[\rho_m^* u_s^* + \langle \rho_1^* u_1^* \rangle]dy^* = const \tag{25}$$

Here, $\rho_m^* u_s^*$ is the net mass flux by the steady component of the second-order axial velocity and $\langle \rho_1^* u_1^* \rangle$ is the net mass flux by the first-order axial velocity and density. For basic and orifice pulse tube refrigerators $\dot{m}_s^*=0$ since the net mass flow rate through a pulse tube is zero. But, the net mass flow rate through a pulse tube is not zero for double inlet pulse tube refrigerators since both ends of the pulse tube are connected by the double inlet valve.[15] According to Wang,[15] who analy zed the double inlet pulse tube refrigerators by a numerical method, the magnitude of the net mass flow rate is about 5% of the amplitude of the periodic mass flow rate.

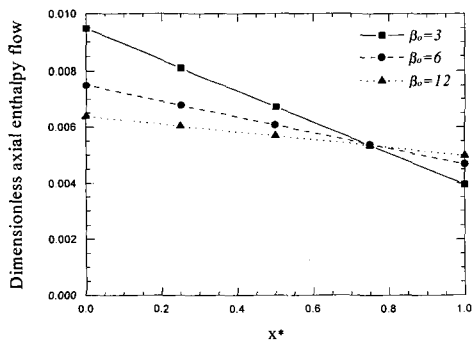

Fig.2 Dimensionless axial enthalpy flow vs. x^* for zero axial temperature gradient. ($s_1/L=0.0875$, Pr $=0.7$, $\gamma=1.4$, $Ma=2\times10^{-4}$, $s_2/s_1=0.3$, $dT_m^*/dx^*=0.6$, $\phi=90^o$)

The second-order energy equation is written in dimensional form to help the understanding of the physical meaning. Integration of the time-averaged second-order energy equation from $y=0$ to $y=H$ gives the following equation.

$$-k\frac{\partial T_s}{\partial y}\Big|_{y=0} = \frac{d}{dx}\int_0^H \rho_m C_p \langle u_1 T_1 \rangle dy + C_p \frac{dT_m}{dx}\int_0^H [\rho_m u_s + \langle \rho_1 u_1 \rangle]dy \tag{26}$$

The second term on the right hand side of equation (26) does not vary with x since the axial temperature gradient, dT_m/dx, is assumed to be constant and the net mass flow rate does not vary with x as shown by equation (25). The term on the left hand side of equation (26) denotes the heat flux from the tube wall to the working gas and can be written as

$$\dot{q}_s = -k\frac{\partial T_s}{\partial y}\Big|_{y=0} = \frac{d\langle \dot{H} \rangle}{dx} \tag{27}$$

where $\langle \dot{H} \rangle$ is the net enthalpy flow rate. From equations (26) and (27) $\langle \dot{H} \rangle$ can be expressed as follows.

$$\langle \dot{H} \rangle = \int_0^H \rho_m C_p \langle u_1 T_1 \rangle dy + C_p \frac{dT_m}{dx}\int_0^H [\rho_m u_s + \langle \rho_1 u_1 \rangle]dy \times x \tag{28}$$

The first term on the right hand side of equation[28] represents the net enthalpy flow rate by the first-order velocity and temperature, and the second term represents the net enthalpy flow rate by steady mass streaming. Net enthalpy flow for basic and orifice type pulse tube refrigerators is generated by the first term since the net mass flow rate is zero. For

no net mass flow rate and adiabatic tube wall, net enthalpy flow by the first-order velocity and temperature, also known as ideal net enthalpy flow, is constant as shown in equation (26). In one-dimensional models of pulse tube refrigerators, only ideal net enthalpy flow is considered.

3. Numerical Method

Complex amplitude of the first-order pressure, $\hat{p}_1^*$, is obtained by numerical integration of the wave equation (6). Fourth-order Runge-Kutta method was used for numerical integration. Using the boundary condition(equation (16)) and assumed value of $\hat{p}_1^*$ at $x^*=0$, equation (6) is integrated up to $x^*=1$. This process is repeated until equation (17) is satisfied. If $\hat{p}_1^*$ is determined, the first-order solutions of velocities, temperature and density can be obtained from equations (2)-(5).

The steady component of the second-order axial velocity, u_s^*, is obtained by numerical integration of equation (23). For the assumed value of dp_s^*/dx^*, equation (23) is integrated from $y^*=0$ to $y^*=1$ using the boundary condition $u_s^*(x^*, y^*=0)=0$ and assumed value of $\partial u_s^*/\partial y^*(x^*, y^*=0)$. Numerical integration of equation (23) is repeated until $\partial u_s^*/\partial y^*(x^*, y^*=1)=0$ is satisfied. dp_s^*/dx^* should be varied until u_s^* obtained from equation (23) satisfies the net mass flow rate equation (25).

4. Results and Discussion

4.1 Ideal net enthalpy flow

Dimensionless ideal net enthalpy flow by the first-order velocity and temperature is given as follows.

$$\langle \dot{H} \rangle_{id}^* = \frac{\langle \dot{H} \rangle_{id}}{\rho_0 C_p \omega s_1 T_H H} = \int_0^1 \rho_m^* \langle u_1^* T_1^* \rangle dy^* \qquad (29)$$

Figure 2 shows the ideal net enthalpy flow for zero axial temperature gradient as a function of x^*. It can be seen that the net enthalpy flow decreases as x^* increases. This trend was also shown by Lee et al.(12) As

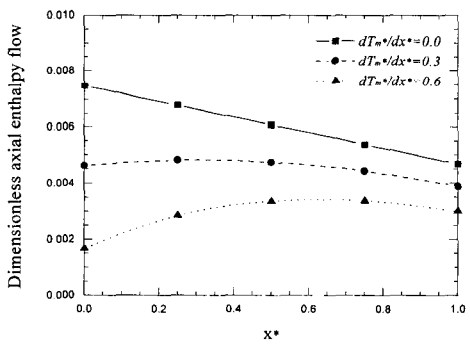

Fig.3 Dimensionless axial enthalpy flow vs. x^* for several axial temperature gradient. ($s_1/L=0.0875$, $\mathrm{Pr}=0.7$, $\gamma=1.4$, $Ma=2\times10^{-4}$, $s_2/s_1=0.3$, $\beta_0=6$, $\phi=90^o$)

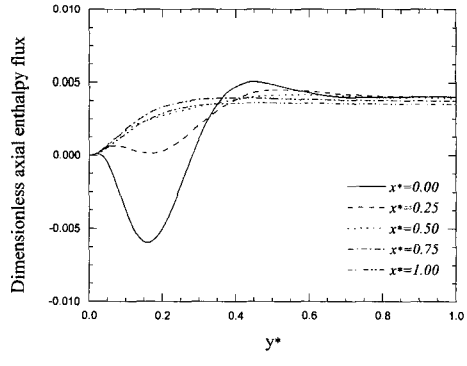

Fig.4 Dimensionless axial enthalpy flux profiles at several x^*'s. ($s_1/L=0.0875$, $\mathrm{Pr}=0.7$, $\gamma=1.4$, $Ma=2\times10^{-4}$, $s_2/s_1=0.3$, $\beta_0=6$, $dT_m^*/dx^*=0.6$, $\phi=90^o$)

β_0 increases, the decreasing rate of the net enthalpy flow decreases.

The effect of axial temperature gradient on the net enthalpy flow is shown in Fig.3. For zero axial temperature gradient, the net enthalpy flow decreases as x^* increases. But, it increases slightly and then decreases after it reaches its maximum for non-zero axial temperature gradient. As the axial temperature gradient increases, the net enthalpy flow decreases, which shows that the cooling capacity of a pulse tube refrigerator decreases as the cooling temperature is lowered.

Figure 4 shows the net enthalpy flux distribution in the direction normal to the wall for $dT_m^*/dx^* = 0.6$. In the region far from the tube wall, the net enthalpy flux is almost uniform and independent on x^*. In the region near the wall, the net enthalpy is transported towards the cold heat exchanger at $x^* = 0$, but transported towards the hot heat exchanger for large x^*. This negative net enthalpy flux in the thermal boundary layer near $x^* = 0$ results in the smaller net enthalpy flow for $dT_m^*/dx^* = 0.6$ as shown in Fig.3.

Figure 5 shows the effect of β_0 on the net enthalpy flow within the pulse tube of a orifice pulse tube refrigerator with $dT_m^*/dx^* = 0.6$ and $s_2/s_1 = 0.3$. Net enthalpy flow increases with x^* near $x^* = 0$, but it decreases after it reaches its maximum. Net enthalpy flow increases with β_0, which means that the refrigeration capacity increases with the frequency of a orifice pulse tube refrigerator. Isothermal wall condition is attained for $\beta_0 \ll 1$, and adiabatic wall condition is attained for $\beta_0 \gg 1$. Larger net enthalpy flow for larger β_0 shows that the cooling mechanism of orifice pulse tube refrigerators is not the 'surface heat pumping' which is the cooling mechanism of basic pulse tube refrigerators.

The effect of velocity ratio, s_2/s_1, on the net enthalpy flow is shown in Fig.6. For basic pulse tube refrigerators $s_2/s_1 \approx 0$, and $s_2/s_1 > 0$ for orifice type or double inlet pulse tube refrigerators. Since the net enthalpy flow for $s_2/s_1 = 0$ is almost zero for all x^* and negative near $x^* = 0$, the basic pulse tube refrigerator

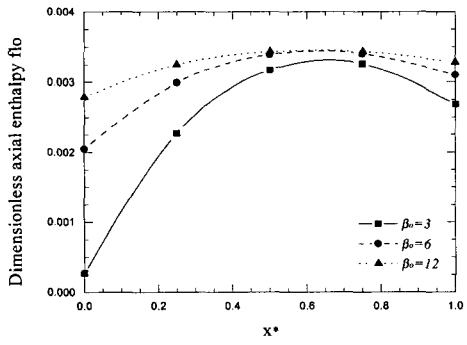

Fig.5 Dimensionless axial enthalpy flow vs. x^* for several β_0's.
($s_1/L = 0.0875$, Pr = 0.7, $\gamma = 1.4$, $Ma = 2\times10^{-4}$, $s_2/s_1 = 0.3$, $dT_m^*/dx^* = 0.6$, $\phi = 90^\circ$)

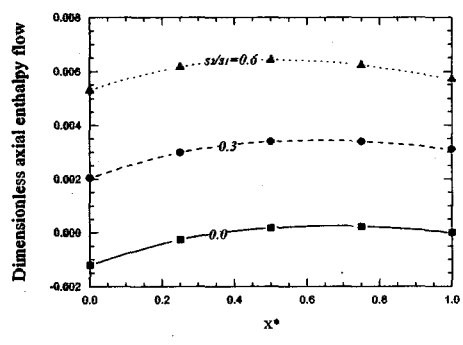

Fig.6 Dimensionless axial enthalpy flow vs. x^* for several s_2/s_1's.
($s_1/L = 0.0875$, Pr = 0.7, $\gamma = 1.4$, $Ma = 2\times10^{-4}$, $\beta_0 = 6$, $dT_m^*/dx^* = 0.6$, $\phi = 90^\circ$)

cannot produce cooling for the operating conditions used in Fig.6. Since the cooling mechanism of basic pulse tube refrigerators is the surface heat pumping due to the heat transfer between the working gas and the tube wall, it seems that $\beta_0=6$ is too large to produce the surface heat pumping effect. Net enthalpy flow increases with s_2/s_1, which infers that the cooling capacities of double inlet pulse tube refrigerators can be larger than those of orifice pulse tube refrigerators.

4.2 Steady mass streaming

Net mass flow rate through a pulse tube is zero for basic and orifice pulse tube refrigerators. Figure 7 shows the net mass flux distribution of a orifice pulse tube refrigerator as a function of the distance from the wall. The gas in the first viscous layer very near the wall and the gas in the core flow towards the cold heat exchanger, but the gas in the second viscous layer between the core and the first viscous layer flows towards the hot heat exchanger. Such a double boundary layer was also shown by Lee et al.(12) As the axial temperature gradient increases the mass flux in the first viscous layer increases, but the mass fluxes in the second viscous layer and the core decrease.

Figure 8 shows the effect of β_0 on the net mass flux. β_0 is the ratio of the distance between the walls to the momentum boundary layer thickness. Hence, larger β_0 means thinner boundary layer thickness. As β_0 increases the thickness of the first viscous layer gets thinner, and the mass fluxes of the second viscous layer and the core increase.

The effect of the velocity ratio, s_2/s_1, on net mass flux is shown in Fig.9. As the velocity ratio increases the first viscous layer becomes thinner and the mass flux in the first viscous layer gets smaller. But, the mass fluxes in the second viscous layer and the core increase as s_2/s_1 increases.

4.3 Enthalpy loss due to steady mass streaming

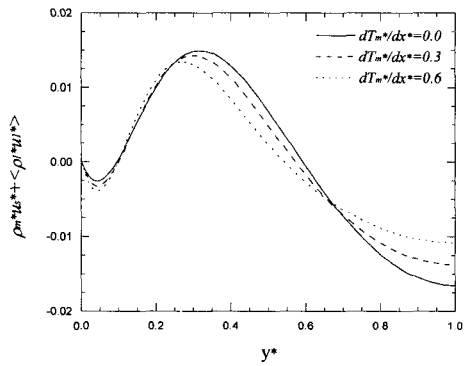

Fig.7 Dimensionless steady mass flux profiles for several axial temperature gradient. ($s_1/L=0.0875$, $\mathrm{Pr}=0.7$, $\gamma=1.4$, $Ma=2\times10^{-4}$, $s_2/s_1=0.3$, $\beta_0=6$, $\phi=90^{\circ}$, $x^*=0.5$)

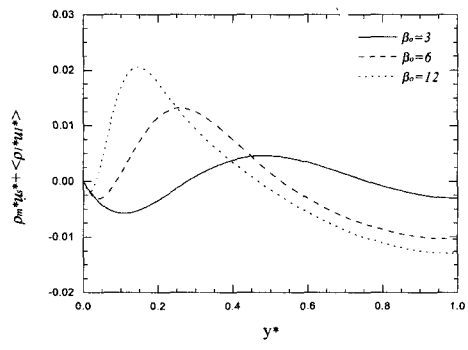

Fig.8 Dimensionless steady mass flux profiles for several β_0's. ($s_1/L=0.0875$, $\mathrm{Pr}=0.7$, $\gamma=1.4$, $Ma=2\times10^{-4}$, $dT_m^*/dx^*=0.6$, $s_2/s_1=0.3$, $\phi=90^{\circ}$, $x^*=0.5$)

Steady mass streaming is caused by the Reynolds stresses inside the momentum boundary layer.[12] For basic and orifice pulse tube refrigerators the net mass flow rate through a pulse tube is zero. This requires that the gas in the core move in a direction counterflow to the gas in the momentum boundary layer to make $\dot{m}_s^*=0$ in equation (25). Hence, there exists no net enthalpy flow due to steady mass streaming for basic and orifice pulse tube refrigerators, which can be inferred from equation (26). However, the steady mass flow rate within the pulse tube of a double inlet pulse tube refrigerator is not zero since both ends of a pulse tube are connected by a double inlet valve. The net mass of the gas will move steadily from the hot heat exchanger to the cold heat exchanger, which is the direction of the mass flux due to Reynolds stresses in the first viscous layer. The major consequences of the mass streaming are the losses associated with a direct enthalpy convection between the cold and warm ends,[8],[12] which reduces the refrigeration capacity. If it is assumed that the ideal net enthalpy flow, which is the first term on the right hand side of equation (28), is constant, the net enthalpy flow rate at the hot heat exchanger will be smaller than that at the cold heat exchanger. The difference is called as the enthalpy loss due to mass or enthalpy streaming, which can be calculated from the following equation.

$$\langle \dot{H} \rangle_{st} = C_p \frac{dT_m}{dx} \int_0^H [\rho_m u_s + \langle \rho_1 u_1 \rangle] dy \times L = \dot{m}_s C_p \triangle T_m \tag{30}$$

Here, $\triangle T_m$ is the temperature difference between the hot and cold heat exchangers.

The effects of the axial temperature gradient and net mass flow rate on the ratio of enthalpy streaming to the ideal enthalpy flow, $\langle \dot{H} \rangle_{st} / \langle \dot{H} \rangle_{id}$, are shown in Fig.10. It can be seen that the enthalpy loss due to mass streaming is proportional to the axial temperature gradient and the net mass flow rate. The enthalpy loss is approximately one order of magnitude smaller than the ideal net enthalpy flow as estimated by Lee et al.[12]

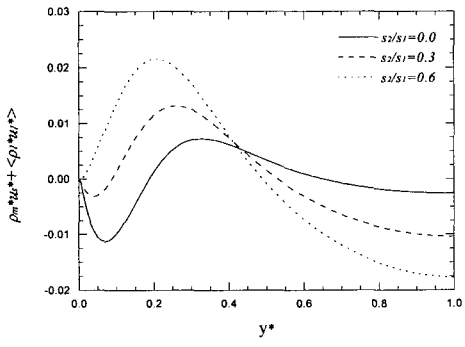

Fig.9 Dimensionless steady mass flux profiles for several s_2/s_1's.
($s_1/L=0.0875$, Pr $=0.7$, $\gamma=1.4$, $Ma=2\times10^{-4}$, $dT_m^*/dx^*=0.6$, $\beta_0=6$, $\phi=90^o$, $x^*=0.5$)

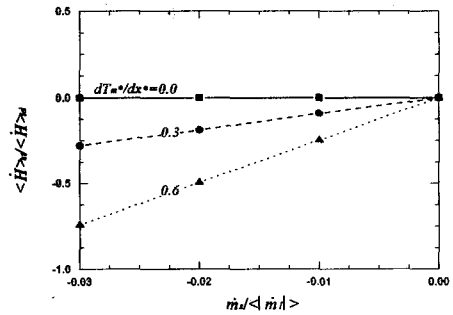

Fig.10 Effects of steady mass flow and axial temperature gradient on the enthalpy streaming loss of DPT.
($s_1/L=0.0875$, Pr $=0.7$, $\gamma=1.4$, $Ma=2\times10^{-4}$, $\beta_0=6$, $s_2/s_1=0.3$, $\phi=90^o$, $x^*=0.5$)

5. Conclusion

In this study, a two-dimensional analysis of a pulse tube was done to include the effects of momentum and heat transfers between the working gas and the tube wall. It was assumed that the axial temperature gradient was constant. Steady second-order conservation equations of mass, momentum, and energy were used to investigate the mass and enthalpy streaming. The effects of the axial temperature gradient, frequency, and velocity ratio on the net enthalpy flow, mass streaming, and enthalpy loss due to the mass streaming were shown.

Ideal net enthalpy flow due to the first-order velocity and temperature decreases as the axial temperature gradient increases, but it increases with the velocity ratio, s_2/s_1, and dimensionless frequency, β_0. The magnitude of the steady mass flux also increases with s_2/s_1 and β_0, but it decreases as the axial temperature gradient increases. For basic and orifice pulse tube refrigerators the enthalpy loss caused by the mass streaming is zero since the net mass flow rate through a pulse tube is zero. However, the enthalpy loss is proportional to the axial temperature gradient and net mass flow rate.

References

(1) Gifford, W. E. and Longsworth, R. C., 1963, "Pulse Tube Refrigeration," *ASME Paper* No. 63-WA-290.

(2) Mikulin, E. I., Tarasov, A. A., and Shkrebyonock, M. P., 1984, "Low Temperature Expansion Tubes," *Advances in Cryogenic Engineering*, Vol. 29, pp. 629-637.

(3) Richardson, R. N., 1986, "Pulse Tube Refrigerator-an Alternative Cryocooler?," *Cryogenics*, Vol. 26, pp. 331-340.

(4) Storch, P. J. and Radebaugh, R., 1988, "Development and Experimental Test of an Analytical Model of the Orifice Pulse Tube Refrigerator," *Advances in Cryogenic Engineering*, Vol. 33, pp. 851-859.

(5) Zhu, S., Wu, P. and Chen, Z., 1990, "Double Inlet Pulse Tube Refrigerators: an Important Improvements," *Cryogenics*, Vol. 30, pp. 514-520.

(6) David, M., Marchael, J. C., Simon, Y. and Guiloin, C., 1993, "Theory of Ideal Orifice Pulse Tube Refrigerator," *Cryogenics*, Vol. 33, No. 2, pp. 154-161.

(7) Wang, C., Ju, Y. L. and Zhou, Y., 1996, "The Experimental Investigation of a Two-Stage Pulse Tube Refrigerator," Cryogenics, Vol. 36, No. 8, pp. 605-609.

(8) Lee, J. M., Kittel, P., Timmerhaus, K. D., and Radebaugh, R., 1993, "Flow Patterns Intrinsic to the Pulse Tube Refrigerator," *Proceedings of the 7th International Cryocooler Conference*, pp. 125-139.

(9) Jeong, E. S. and Smith, J. L., Jr., 1992, "Secondary Flow in Reciprocating Machinery," *Proceedings of ASME National Heat Transfer Conference*, Vol. 24, pp. 97-104.

(10) Jeong, E. S., 1996, "Secondary Flow in Basic Pulse Tube Refrigerators," *Cryogenics*, Vol. 36, No. 5, pp. 317-323.

(11) Lee, H. J., Chae, W. B. and Jeong, E. S., 1997, "Second-Order Velocity and Temperature in Pulse Tube Refrigerators," *Korean Journal of Air-Conditioning and Refrigeration Engineering*, Vol. 9, No. 2, pp. 239-248.

(12) Lee, J. M., Kittel, P., Timmerhaus, K. D., and Radebaugh, R., 1995, "Steady Secondary Momentum and Enthalpy Streaming in the Pulse Tube Refrigerator," *Cryocoolers* 8, Plenum Press, New York.

(13) Liang, J., Ravex, A., and Rollang, P., 1996,

"Study on Pulse Tube Refrigeration Part 2: Theoretical modelling," *Cryogenics*, Vol. 36, No. 2, pp. 95-99.

(14) Lee, J. M., Kittel, P., Timmerhaus, K. D., and Radebaugh, R., 1996, "Useful Scaling Parameters for the Pulse Tube," *Advances in Cryogenic Engineering*, Vol. 41, pp. 1347-1355.

(15) Wang, C., 1997, "Numerical Analysis of 4K Pulse Tube Coolers: Part II. Performance and internal Processes," *Cryogenics*, Vol. 37, No. 4, pp. 215-220.